Separation of lipids and proteins from clarified microalgae lysate: The effect of lipid-protein interaction on the cross-flow and shear-enhanced microfiltration performances

Shuli Liu, Camille Rouquié, Matthieu Frappart, Anthony Szymczyk, Murielle Rabiller-Baudry, Estelle Couallier

Separation of lipids and proteins from clarified microalgae lysate: The effect of lipid-protein interaction on the cross-flow and shear-enhanced microfiltration performances

Shuli Liu[a,b], Camille Rouquié[c], Matthieu Frappart[a], Anthony Szymczyk[d], Murielle Rabiller-Baudry[d], Estelle Couallier[a,*]

[a] Nantes Université, CNRS, ONIRIS, Laboratoire de Génie des Procédés, Environnement et Agroalimentaire, GEPEA, F-44600, Saint-Nazaire, France

[b] Agence de l'environnement et de la Maîtrise de l'Energie, 20 avenue du Grésillé-BP 90406, 49004, Angers Cedex 01, France

[c] INRA, BIA, Rue de la Geraudière, BP 71627, 44316, Nantes Cedex 3, France

[d] Univ Rennes, CNRS, ISCR (Institut des Sciences Chimiques de Rennes) - UMR 6226, F-35000, Rennes, France

Corresponding author: estelle.couallier@univ-nantes.fr

https://doi.org/10.1016/j.seppur.2023.124985

Received 21 May 2023; Received in revised form 29 August 2023; Accepted 30 August 2023

Abstract

For microalgae biorefinery, membrane process is a suitable technology for biomolecules (i.e., proteins, lipids or carbohydrates) fractionation due to the simplicity in operation, the flexibility for implementation and the potential for processing large volumes. Here the objective was to microfiltrate microalgae aqueous extracts, after cell disruption and clarification, to concentrate lipids in retentate and recover hydrophilic proteins in permeate. However, the optimization of the membrane process requires a large amount of raw material and the composition of real microalgae extracts is so complex that it limits the in-depth understanding of the membrane / molecules interactions on the modification of the filtration performances. Thus, simplified model mixtures of clarified microalgae lysates were formulated, aiming at quite a high complexity with constant composition but a nice representativity with respect to the real mixture. Through the microfiltration of three model mixtures containing lipids, proteins or both kinds of molecules, it was demonstrated that the strong interaction between the biomolecules in solution modified the membrane fouling and had a clear impact on the

membrane permeation and selectivity, similarly to the real mixtures. The dynamic filtration was tested to enhance the performances compared to cross-flow filtration. The higher shear rate favored an increase in flux and therefore productivity, but did not modify membrane selectivity. It was therefore demonstrated that the interaction between molecules existing in the cell or generated during the cell disruption drives the separation efficiency and should be mitigated in future works to allow the whole biomass biorefining.

Keywords

Cross-flow filtration, shear-enhanced filtration, microalgae biorefinery, lipids proteins interaction, Oil-in-water emulsion

1. Introduction

Nowadays, microalgae cultivation and valorization have become an attracting research topic as its potential has been successfully demonstrated in various sectors, such as energy, cosmetics, pharmaceutics, food and feed. Intensive research has been performed for the optimization of microalgae production [1–5]. Several microalgae strains, *Chlorella vulgaris* for example, are rich in proteins and are considered as a new protein resource for food and feed. Other strains, like *Parachlorella kessleri*, were identified as able to enhance the lipid storage under specific culture conditions, these lipids has a great potential for biofuel conversion after extraction [6–8].

The microalgae biorefinery in wet processing was proposed by several authors [9–12] in order to avoid the conventional biomass drying step before extraction, which is either high energy consuming or physical-biological properties affecting. The eco-friendly wet processing involves four major operations: the harvesting step to concentrate the biomass and to recycle the culture medium, the biomass cell disruption to release the intracellular compounds in the aqueous phase, the clarification of the microalgae extract to remove the solid cell fragments, and the final separation to fractionate and purify the hydrophobic (lipids and parts of pigments) and hydrophilic compounds (ash, soluble proteins and carbohydrates).

Considering cell disruption, the bead milling has been deeply studied due to its high efficiency at high biomass concentrations (30-100 $g \cdot L^{-1}$) [13,14]. For the separation of biomolecules dispersed in the remaining aqueous phase after bead milling, membrane processing is a suitable technology due to the simplicity in operation (without solvent use), the flexibility for implementation (wide range of materials, cut-off and geometries) and the potential for large volume treatment [15,16]. Several studies on microalgae biorefinery

downstream processes have been focused on the membrane separation or purification process [14,17–19]. The ultrafiltration membranes with a molar weight cut off up to 300 kDa were mostly used to concentrate the biomolecules from the aqueous extract. But when the objective is to let the hydrophilic compounds permeate through the membrane, the performances are much lower, most of the lipids are fully retained up to 100 %, but the protein recovery yields in the permeate is very low (retention rate above 80 %), even with microfiltration membranes. This can be related to the difficulty of coupling bead milling (BM) and membrane filtration. Indeed, during BM process for cell disruption, the applied mechanical force has no specific destruction target. As a consequence, the release of amphiphilic molecules (proteins, polar lipids, etc.) and neutral lipid droplets (triacylglycerides, free fatty acids) in the presence of high shear rate brings together the conditions to produce a stable emulsion [20–23]. This new stable system composed of complex colloidal structures will become a major obstacle in the downstream separation and purification.

Thus, the key point to optimize the coupling of BM and membrane processes is to understand the nature of the released compounds, the interactions between the compounds and compounds/membrane under processing conditions, and how these interactions impact the filtration performances (selectivity and permeation flux).

The deepening of the impact of the composition of the complex aqueous microalgae extracts on the microfiltration performances necessitates large volumes of extracts corresponding to several m^3 of microalgae cultures. The production of such large quantities of microalgae aqueous extracts would necessitate both high investment and skilled labor, especially in the case of strains cultivated in starving conditions to orientate their metabolism (like *Parachlorella kessleri* to produce lipids). The current cultivation processes do not allow to fulfill these criteria. Moreover, the different batches of biomass and their storage would induce variability in the filtered solution as deduced from already available characterizations (composition, organization, etc.) [13,22]. Thus, in this work, the strategy was to elaborate controllable model mixtures with an increasing complexity to deepen the study of the interaction and their impact on the process.

The objective was to study the impact of the lipid-protein interactions on the performances of the microalgae extracts microfiltration, using accessible methods to go towards local understanding. Three model mixtures were formulated with composition close to real microalgae extracts, containing only proteins (MM_P), only lipids (MM_L) or both ($MM_{P/L}$), and characterized by electrophoresis and particle size distribution. Then they were filtrated with a

polyethersulfone (PES) membrane with a mean pore diameter of 0.1µm, the performances were compared to the filtration of real microalgae extracts, and the fouling characterized using fouling resistance measurement and ATR-FTIR. The impact of the interaction between proteins and lipids on membrane filtration performances was highlighted (retention rate, flux, fouling characterization). The effect of the filtration hydrodynamics on the membrane permeability and the selectivity with such complex mixtures was also investigated.

2. Materials and Methods

2.1. Preparation of the model mixtures

The model mixture preparation included three steps: the aqueous phase preparation, the oily phase preparation and the emulsification process.

2.1.1. Aqueous phase preparation

For MM_L, the aqueous phase contained only a diluted phosphate buffer (pH 7.4, Conductivity 790 $\mu S \cdot cm^{-1}$, close to *Parachlorella kessleri* culture medium properties). For MM_P and $MM_{P/L}$, the selected vegetable protein product was firstly dispersed at 12.5 $g \cdot L^{-1}$ in phosphate buffer (pH 7.4, Conductivity 790 $\mu S \cdot cm^{-1}$) and continuously stirred at 700 rpm for 24 hours at room temperature to reach maximum solubilization. Then the soluble protein fraction was recovered by centrifugation at 12 000 *g* for 15 min and the soluble protein concentration was adjusted at 0.7 $g \cdot L^{-1}$ by the addition of a phosphate buffer.

2.1.2. Oily phase preparation

A concentrated lipid phase was prepared to ensure the appropriate polar and neutral lipids' balance as follows: 2.6 g lecithin extract and 17.4 g vegetable oils were homogenized using an ultrasonic processor (VCX130 PB Vibra-Cell™, Sonics, USA) at 65 % amplitude for 6 min.

2.1.3. Emulsification process

First of all, the appropriate volume of the lipid phase was added to the aqueous in order to achieve a protein/lipid concentration ratio of 1/2, and this solution was pre-emulsified by a rotor-stator T25 homogenisator (T25 Digital ULTRA-TURRAX®, IKA®, Germany) at 10 000 rpm during 2 min to avoid the oily phase float on the surface of the aqueous phase during the emulsification. Then it was emulsified with a continuous rotor-stator T18 (T18 Digital ULTRA-

TURRAX®, IKA®, Germany) at 19 000 rpm for 45 min. The stability of the model mixtures after preparation was followed by granulometry (Mastersizer 3 000, Malvern Panalytical, UK).

2.2. Real and model mixtures characterization technics

The dry matter was determined by drying the samples up to constant mass in an oven at 105 ± 5 °C. The soluble proteins were quantified by a BCA Protein Assay kit (Thermo Scientific) (the proteins suspended in the supernatant at 12 000 *g* were named "soluble" even if colloids can be present). The total lipids were determined by a gas chromatography-flame ionization detector and polar lipid classes were quantified by a high-performance thin-layer chromatography [22].

The emulsion droplet size distributions were analyzed by a MASTERSIZER 3000 size analyzer (Malvern Panalytical, UK), the particles refractive index was set at 1.47 for MM_P and $MM_{L/P}$, at 1.465 for MM_P and at 1.430 for the real mixtures from *Parachlorella vulgaris*. The particulate absorption index was set at 0.01[24–27].

Two types of electrophoresis, Native-PAGE (Native PolyAcrylamide Gel Electrophoresis) and SDS-PAGE (Sodium DodecylSulphate PolyAcrylamide Gel Electrophoresis) were carried out to determine the molecular weight of the native proteins and their subunits. The Native-PAGE was performed with a 12 % native polyacrylamide handmade gel with 10-1 200 kDa NativeMark Unstained protein standard (ThermoFisher). For SDS-PAGE, the proteins were denatured in a SDS sample buffer at 95 °C during 3 min; for electrophoresis, a Bolt™ 10 % Bris-tris Plus Gels and 40-300 kDa Spectra™ Multicolor High Range Protein Ladder standard (ThermoFisher) were used.

All the values resulting from the samples analysis (dry matter, lipids and proteins analysis) were calculated by the means of triplicate measurements. The standard errors (SE) presented in the results were calculated as the standard deviations of the triplicate divided by √3. The combined standard error of any y value was calculated by Equation 1 for additions or Equation 2 for multiplications or divisions of two variables X_1 and X_2:

If $y = X_1 + X_2$,

$$SE_y = \sqrt{SE_{X1}^2 + SE_{X2}^2} \qquad \text{Equation 1}$$

If $y=X_1^{\pm 1} \times X_2^{\pm 1}$,

156 $$SE_y = y.\sqrt{\left[\frac{SE_{X1}}{X1}\right]^2 + \left[\frac{SE_{X2}}{X2}\right]^2}$$ Equation 2

157 **2.3. Membrane filtration**

158 *2.3.1. Cross-flow filtration pilot*

159 The membrane with an effective filtering area of 130 cm^2 was mounted in a Rayflow
160 X100 module (Rhodia, Orelis) equipped with a 1.5 mm sealing gasket corresponding to the
161 liquid channel thickness. The cross-flow filtration was performed thanks to a peristaltic pump
162 (Masterflex I/P77600-62, Cole Parmer, USA). A valve on the retentate outlet pipe allows
163 mastering the transmembrane pressure (TMP), calculated as the average of the pressions at the
164 inlet and outlet measured by 2 pressure sensors (± 0.01 bar). The feed solution temperature was
165 maintained with a regulated warming plate. In order to enhance the back-transport mechanisms
166 near the membrane surface, a spacer of 1.5 mm (reference 46 mil) was used and the apparent
167 cross-flow velocity was estimated at v_{app}=0.8 $m.s^{-1}$. The permeate was continuously weighted
168 to measure the permeate flow (+/- 1-3% in DF and 5-8% in CF due to the peristaltic pump).
169 All the data were collected with a Labview software.

170 *2.3.2. Rotating disc filtration pilot*

171 The dynamic filtration experiments were carried out using a rotating disk dynamic
172 filtration system. As described by Frappart et al. 2011 and Bouzerar, Ding, et Jaffrin 2000
173 [29,30], the membrane was installed into the cylindrical chamber in front of the disk, and the
174 effective membrane area was 188 cm^2. The feed (stirred and temperature controlled) was sent
175 to the filtration module by a peristaltic pump (Masterflex I/P77600-62, Cole Parmer, USA).
176 The peripheral pressure (Pc) was adjusted by a valve on the retentate outlet and measured at the
177 top of the cylindrical housing by a pressure sensor. Rotational disk speed could be adjusted
178 from 0 to 3 000 rpm, and the disk was equipped with radial vanes. The shear rate was calculated
179 as a function of rotation velocity and disk profile as described by Bouzerar, Ding, et Jaffrin
180 2000 [30] (Equation 3).

181 In order to study the impact of hydrodynamic conditions on the filtration performances,
182 two hydrodynamic conditions were tested in DF: 16 000 s^{-1} (γ_1) and 66 000 s^{-1} (γ_2).

183 $$\gamma = 0.0296 r^{8/5} (k\omega)^{9/5} v^{-4/5}$$ Equation 3

Where: ω is the disk angular velocity (rad s^{-1}), k is the velocity factor which was 0.89 in our case for a disk equipped with 6 mm vanes, ν the kinematic viscosity ($m^2 \cdot s^{-1}$) and r the distance from the center, where the maximum shear rate value for tested two hydrodynamic conditions γ_1 and γ_2 were calculated with the disk radius equal to 0.0725 m, at the membrane periphery.

2.3.3. Membrane preparation prior filtration

For each experiment, a new organic microfiltration membrane PES 0.1µm (K618, KOCH Membrane Systems, USA) was previously conditioned as follows: it was rinsed with deionized (DI) water to remove the preservative, cleaned with 100 ppm chlorine solution under alkaline conditions (pH 10) for 30 min at room temperature (23 °C), then cleaned with 0.2 $\%_{v/v}$ Ultrasil 110 (Ecolab, USA) for 30 min at 45 °C, and finally rinsed with DI water during 35 min. after the cleaning and before filtration, the membrane was compacted at 30 °C under a transmembrane pressure TMP of 1 bar until the permeate flow was stabilized. The membrane initial water permeability was measured for each coupon, before each filtration.

Due to the heterogeneity of the membrane material different values of the water permeability were observed on the different membrane 130 cm^2 coupons of a same lot of PES membranes, which was in accordance with the membrane pore size distribution obtained by scanning electron microscopy (the majority of the pores had a diameter between 50 and 110 nm for the membranes with a higher water flux, and between 20 and 50 nm for the others). Therefore, during the flux results analysis, the permeate flux was always normalized to the initial DI water flux of the membrane before filtration.

2.3.4. Filtration of MM and RM

2.3.4.1. Determination of critical conditions with MM

First of all, in order to limit the membrane overall fouling during the set of experiences in concentration mode (increasing volume reduction ratio VRR), the critical pressure of the most complex model mixture $MM_{P/L}$ was determined both in CF and in γ_1 hydrodynamic conditions for DF. The critical pressure, corresponding to the lowest TMP to avoid high irreversible fouling in given hydrodynamic conditions, was determined in batch mode with full recycling of both retentate and permeate to the feed tank (30 °C). The dry matter concentration was thus maintained constant and VRR=1 was remained. Accordingly, TMP was voluntary gradually increased from 0.1 to 0.5 bar for CF and from 0.1 to 1 bar for DF (0.1-0.2 bar each

step). The stabilized permeate flux was measured for each TMP. The critical conditions (critical TMP, critical flux) were deduced from the Jp vs TMP plot and correspond to the last point belonging to the first linear part of the plot. The critical pressure was 0.50 bar for CF and 0.54 for DF, respectively.

2.3.4.2. Filtration in concentration mode below critical TMP

The concentration process was carried out with 3L of the solution at 30 °C regardless of CF or DF filtration mode, the VRR was increased up to 3 as follows: the retentate was fully recycled into the feed tank while the permeate was continuously extracted. The working TMP was chosen at 90 % lower than the critical pressure and set at 0.45 bar for CF and 0.50 bar for DF. For each filtration samples of the feed, retentate and instantaneous permeate were regularly collected and subsequently analyzed. Two hydrodynamic conditions were tested for DF (γ_1 at 16 000 s^{-1} and γ_2 66 000 s^{-1}): γ_1 was used for each model mixture, and only $MM_{P/L}$ was also filtrated with γ_2 to understand the impact of the shear stress increasing. Each experiment with model mixtures was repeated at least twice. For RM, a subcritical TMP of 0.30 bar was selected for both CF and DF according to previous determination and following a similar protocol. RM was filtrated once in CF and once in DF under γ_1 hydrodynamic condition as well to compare with the results of MM.

2.3.5. Membrane rinsing and cleaning after MM and RM filtration.

After filtration, a simple water rinsing with 5 L at 30°C in an open circuit was carried out in order to remove the physically reversible fouling, then the membrane water permeability was measured to determine the fouling resistance R_f including both the chemically reversible (removed by chemical cleaning) and the irreversible (remaining after cleaning) fouling (Equation 4).

$$R_f = R_t - R_m = \frac{TMP}{\mu}\left(\frac{1}{J_{wf}} - \frac{1}{J_{wi}}\right) \quad \text{Equation 4}$$

Where: R_t represents the total resistance calculated from water permeability measurement (water flux J_{wf}) after the concentration experiment and the water rinsing, and R_m the membrane resistance calculated by water permeability measured on the pristine membrane (water flux J_{wi}).

After rinsing, the membrane was removed from the pilot and prepared for the subsequent membrane fouling characterization.

2.4. ATR-FTIR membrane fouling characterization

The membrane lipids fouling accumulation was characterized by ATR-FTIR. Membrane samples were carefully dried under dynamic vacuum at least three days before ATR-FTIR registration, in order to remove adsorbed water and avoid the corresponding absorption band (large band around 3300 cm^{-1} and harmonic band at 1660 cm^{-1}).

For the sake of accuracy, several spectra were registered for each membrane. For cross-flow, the mean value of 4 spectra measured in the center of the membrane is depicted in the results. For dynamic filtration, the values from the center of the membrane, the intermediate annular and the external annular bands are shown each one corresponding to the average of 4 spectra (see Figure 5).

The ATR-FTIR spectra were registered with a Spectrum 100 (Perkin Elmer) spectrometer using the Spectrum for Windows software (5.3) either for data acquisition or spectra treatment. The spectrometer was equipped with an ATR accessory having a diamond monoreflexion crystal (1.8 mm size) with an incidence angle of 45°. The background was recorded in the air and each spectrum was the accumulation of 20 scans with 2 cm^{-1} resolution in the 4000-600 cm^{-1} range. The band height H^x at the x wavenumber were then measured on the raw spectra after setting the baseline between 2240 and 2060 cm^{-1} (region without any absorption bands of the membrane) adapting the procedure reported in [31,32].

In absence of calibration which is too long to establish, semi-quantification was carried out inspired by the methodology proposed by *Delaunay et al. 2008* for protein quantification [33] and as reported in [31,32]. The relative concentration of lipids deposited on the membrane was evaluated through calculation of $\frac{H_{lipids}}{H_{PES}}$ ratios, H_{lipids} being a band of high intensity typical of the lipids of the oil-in-water emulsion and H_{PES} being a band of high intensity typical of PES used as internal standard. H_{lipids} was set at 1744 cm^{-1} (C=O stretching, fatty acid triglycerides or phospholipids esters), and H_{PES} was selected at 1576 cm^{-1} (C=C) for PES membrane both being of high intensity and without any overlapping.

3. Results and Discussion

3.1. Formulation of the model mixtures

3.1.1. Selection of the model mixtures ingredients

3.1.1.1. Neutral and polar lipids in model mixtures

In the supernatant obtained from nitrogen starved *Parachlorella kessleri* after cell disruption and centrifugation, the total lipids of the supernatant contain around 46% triacylglycerides (TAG), 44% other neutral lipids (mainly free fatty acids FFA), and 10% of polar lipids (6% glycolipids and 4% phospholipids) playing the role of an emulsifier [22]. In model mixtures, a blend of vegetable oils was formulated to represent the neutral lipids (mostly TAG) present in the discontinuous oily phase of a real mixture [34].

Polar lipids, especially phospholipids are natural amphiphilic molecules and are the major compounds of the cell membrane. Phospholipids are commonly used as emulsifiers because they have hydrophobic fatty acid tail groups and hydrophilic head groups containing phosphoric acid esterified with glycerol and other substitutes [35]. Under oil-in-water (O/W) emulsion, the high flexibility of phospholipids due to their small size and clearly defined two opposite affinity parts, promote a rapid interface arrangement compared to proteins [21].

To represent the polar lipids (phospholipids and glycolipids), a lecithin extract from soybeans (VWR CHEMICALS, USA) which contains 97.6%$_{DM}$ of polar lipids and 2.4%$_{DM}$ of proteins was selected based on the polar lipids compositions and purity of this product.

The comparison of the polar lipids characteristics between the real mixture – the supernatant – and lecithin extract is presented in Table 1. The supernatant contains two main families of polar lipids with surfactant properties: glycolipids and phospholipids. For the phospholipids fraction, the supernatant contained mainly 28 % PC and 13 % PI, compared to the 31 % PC and 38 % PI for the lecithin extract, while for glycolipids, 7 % MGDG and 9 % DGDG for the supernatant and 14 % and 1 % for the lecithin extract.

Despite those inevitable differences between the two bioresources, to ensure a stable emulsion system, the lecithin extract was chosen as an appropriate model of lipid-based emulsifier for model mixtures formulation. The ratio between neutral lipids (TAG from vegetable oils blend) and polar lipids (Lecithin) in model mixture was fixed as 87 % neutral lipids and 13 % polar lipids, similar to the proportion in the supernatant (90 % neutral lipids and 10 % polar lipids).

*Table 1. Characteristics of polar lipids from supernatant and lecithin extract**

Full name	Abbreviation	Supernatant	Lecithin extract	
		g·g^{-1} polar lipids	g·g^{-1} polar lipids	% DM
Lysophosphatidycholine	LPC	11	8.0 ± 2.4	7.8 ± 2.4
Phospatidylcholine	PC	28	31.6 ± 0.9	30.8 ± 0.9
Phospatidylinositol	PI	13	38.7 ± 1.0	37.8 ± 1.0
Cardiolipid	CL	6	0.7 ± 0.1	0.7 ± 0.1
Phosphatidylethanolamine	PE	1	DT	DT
Phosphatidylglycerol	PG	2	DT	DT
Sulfoquinovosyldiacylglycerol	SQDG	23	DT	DT
Sphingomyeline	SM	DT	0.7 ± 0.4	0.7 ± 0.3
Monogalactosyldiacylglycerol	MGDG	7	13.8 ± 4.2	13.5 ± 4.1
Digalactosidediacylglycérol	DGDG	9	1.3 ± 0.1	1.3 ± 0.1

* DT: detected, no standard for quantification.

3.1.1.2. Proteins in model mixtures

The proteins, which are macromolecules with various functions in the microalgae cells, are more difficult to characterize. The hydrophobic or hydrophilic groups in proteins are determined by the primary sequence of the amino acids, some of them being exposed or hidden with respect to the tertiary structure folding and even their quaternary structure corresponding to aggregation in soluble state. However, this native conformation can be modified by hydrogen bonds, hydrophobic interactions and ion–ion interactions with substances of their physico-chemical environment [36]. Microalgae proteins contain an important ratio of amino acids with hydrophobic side groups as isoleucine, phenylalanine and leucine [37]. In an O/W emulsion, amphiphilic proteins may adsorb onto an oil-water interface, reorganize their hydrophobic groups into oil droplets and hydrophilic groups into the aqueous phase [21]. In consequence, the protein molecules may partially be denatured or unfolded during the reorganization [21,38,39]. Accordingly, the variation of the conformation is protein dependent and would strongly depend on the fraction of hydrophobic amino acids (number and spatial repartition in the primary sequence) and on the surface of interactions with the outer environment that result from complex equilibria.

Since the amino acid profile of proteins from *Parachlorella kessleri* was not described in literature, the protein extracts from microalgae *Chlorella vulgaris, Dunaliella tertiolecta* and *Nannochloris atomus*, with the same chlorophyte phylum as *Parachlorella kessleri*, were compared with a selection of vegetable proteins available in appropriate quantity on the market.

An organic vegetable protein product was then selected. The amino acid profiles are compared in Figure 1. Microalgae contain an important ratio of leucine (Leu), phenylalanine (Phe), isoleucine (Ile), amino acids with amphiphilic properties [21,37–39]. The selected vegetable protein product contains these amino acids in similar proportions and was selected accordingly. This selected vegetable protein source contains 85 % proteins, 9.4 % lipids, 0.9 % fibers and less than 0.5 % carbohydrates. The soluble proteins were extracted to represent the soluble proteins from a real mixture (supernatant).

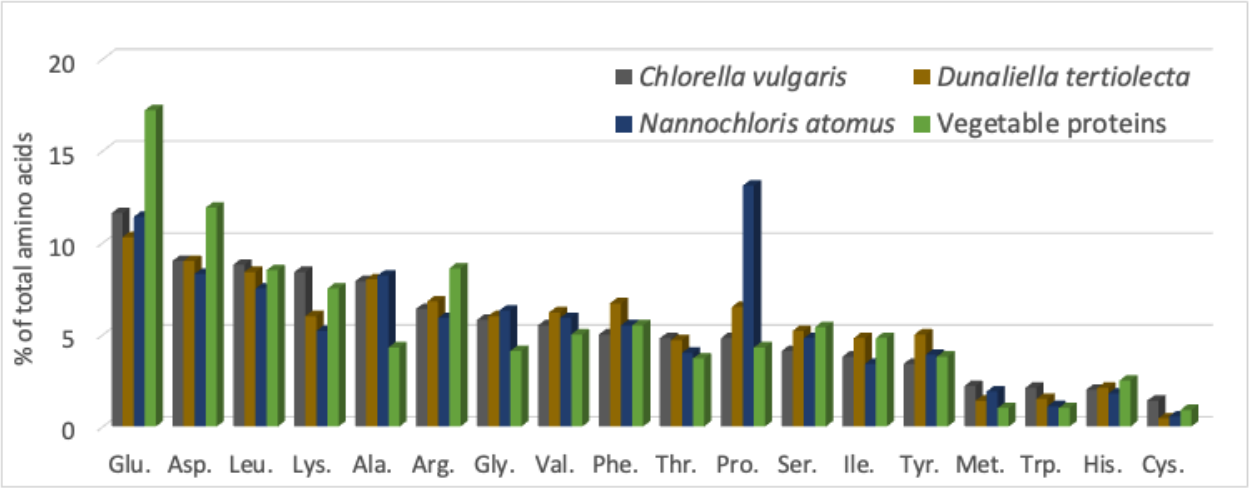

Figure 1. Amino acid profile comparison between microalgae and vegetable proteins.(Becker, 2007)

3.1.2. Model mixture formulation strategy

The composition of the real mixture (RM) and the model mixture (MM) are described in Table 2. The RM were the supernatant fraction recovered after the bead milling and centrifugation 3000 *g* of a *Parachlorella kessleri* biomass at 3.7 $g{\cdot}L^{-1}$ of dry matter. RM contains 0.31 $g{\cdot}L^{-1}$ of lipids, 0.20 $g{\cdot}L^{-1}$ of proteins and 0.72 $g{\cdot}L^{-1}$ of carbohydrates. The proportions of proteins, lipids and carbohydrates in RM are from the expected ones [40] and could be related to difficulties in the culture of *Parachlorella kessleri* in starving conditions at a large scale.

It was demonstrated that a bead milling at a higher biomass concentration is more energetic efficient (up to 100 $g{\cdot}L^{-1}$)[13]. However, in this work, the experiments of RM with higher biomass concentration could not be realized due to the limitation of biomass feedstock. Therefore, the MM was specifically set to be more concentrated than RM but the same lipids-proteins ratio was preserved in MM as in RM. The concentrations of lipids and soluble proteins were 5 times higher than in RM not only to mimic microalgae extracts obtained after the bead

milling at a higher concentration, but also to simulate the performance of the membrane under harsher conditions. As shown in Table 2, MM_L contains around 0.15 $\%_{w/v}$ mixture of neutral and polar lipids, MM_P contains 0.075 $\%_{w/v}$ soluble vegetable proteins and $MM_{P/L}$ contains 0.15 $\%_{w/v}$ of total lipids and 0.075 $\%_{w/v}$ soluble vegetable proteins.

The RM also contain carbohydrates but their nature and quantity strongly varies depending on the culture conditions. It was chosen as a first approach not to introduce such a fraction in the MM because these biomolecules are not currently well described. The development of a corresponding MM would necessitate a deep characterization of the complex carbohydrates contained in the considered microalgae, which have been limited by time in this study. However the comparison between RM and MM have brought indirect understanding on their potential role.

*Table 2. Comparison of formulated model mixtures (MM) compositions with real mixtures (RM)**

	Measurement			
	DM	Lipids	Soluble proteins	Carbohydrates
	$g \cdot L^{-1}$	$g \cdot L^{-1}$	$g \cdot L^{-1}$	$g \cdot L^{-1}$
MM_L	2.5±0.2	1.43±0.02	-	0
MM_P	2.0±0.2	-	0.70±0.10	0.07
$MM_{P/L}$	3.6±0.2	1.41±0.02	0.70±0.10	0.07
RM	2.5±0.1	0.31±0.01	0.20±0.01	0.72

*RM: Real mixtures were the supernatants from bead milling and centrifugation of the biomass *Parachlorella kessleri* 3.7 $g \cdot L^{-1}$ (ash-free dry matter). DM presented in the table are total dry matter including ash. (-) measured, not detected.

3.1.3. Comparison of the model mixtures and microalgae extracts

After model mixtures formulation, the composition and the organization of the compounds in the model and real mixtures were compared using different characterization technics as described in 2.3.

3.1.3.1. Particle size distribution

Figure 2 compares the particle volume size distributions between the real mixture and the model mixtures before and during filtration, measured by granulometry on Mastersizer 3000. Regarding the real mixture RM, the particle size mainly ranged from 0.01 to 2.0 µm, some large objects, around 10-100 µm, were also detected, which may be the cell fragments recovered in the supernatant or aggregates after centrifugation. Regarding the particle size of MM_L containing only polar and neutral lipids, the particles were distributed between 0.1-10

µm, with two main modes at 0.5 µm and 2.9 µm, corresponding for the smallest to micelles or vesicles of polar lipids, and for the largest to O/W droplets. For MM_P, the main mode was at 18 µm, which means a part of the proteins were aggregated into large particles and were not eliminated by the former centrifugation. The free proteins can not be measured with the granulometry method. The aggregation was also observed by Linder, 2009 and Stradner et al., 2004 [41,42]: they observed that the proteins form monolayers like supramolecular clusters and micelles in aqueous bulk phases. Surprisingly, in $MM_{P/L}$, with mixture of soluble proteins, polar lipids and neutral lipids, the particle volume size distributions showed mainly two modes at 0.4 µm and 2.5 µm, smaller than the aggregates in MM_P. The protein-lipid mixture is milky white and opaque, but clear and homogeneous.

According to Courthaudon et al., 1991; Damodaran, 2005 and Euston et al., 1995 [21,43,44], when polar lipids, like lecithin, and proteins are mixed together as emulsifiers before emulsification process, those molecules compete with each other for adsorption on the O/W interface and form multi-emulsifier micelles. This competitive adsorption varies with the type and ratio of the two emulsifiers. Their interaction (competition or coexistence) will impact the characteristics of the emulsion droplets. According to the particle size distributions of the model mixtures, it appears here that the large protein aggregates were dissociated. They could be either on the lipid droplets, in micelles or partially dissolved. However the particle size distribution of the $MM_{P/L}$ is the nearest of the RM one. Thus a clear interaction between proteins and lipids was highlighted in $MM_{P/L}$.

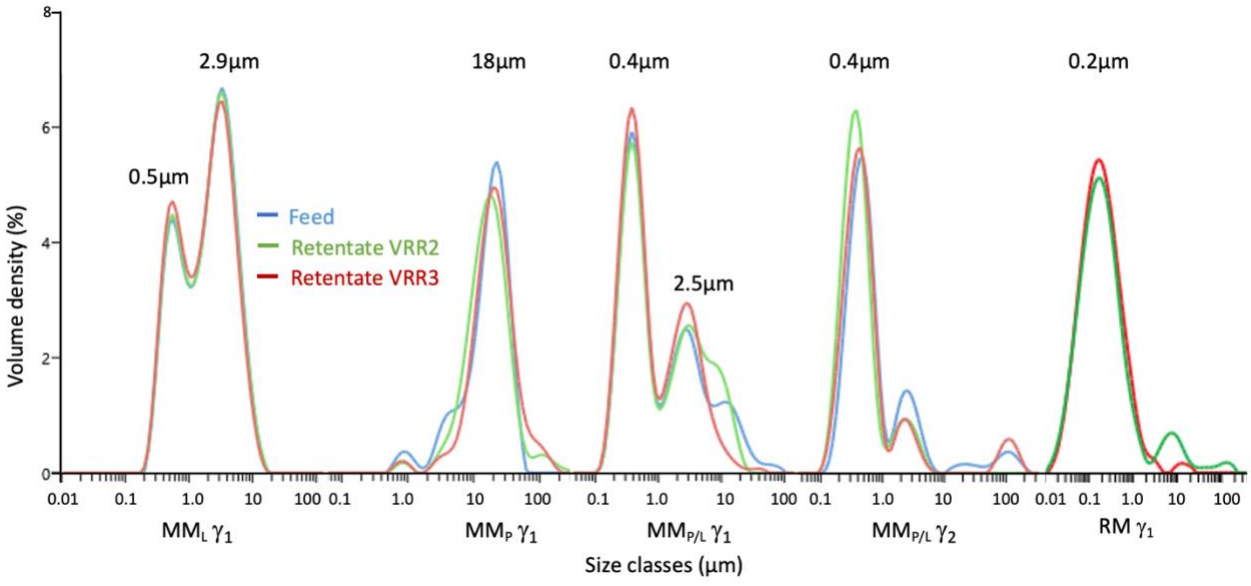

Figure 2. Particle size volume distribution comparison between model mixtures and real mixtures before and during rotating disc filtration. MM: Model Mixture, RM: Real mixture, γ: filtration hydrodynamic conditions γ_1 at 16 000 s^{-1} and γ_2 66 000 s^{-1}

3.1.3.2. Electrophoresis analysis

In this paragraph, the objective is to verify if the vegetable protein is an acceptable model for microalgae proteins. Figure 3 shows the results of electrophoresis in Native-PAGE and SDS-PAGE in order to compare the proteins and their subunit sizes between extracted vegetable proteins and microalgae proteins. According to Alavijeh et al., 2020; Günerken et al., 2016; Teuling et al., 2017 [45–47], microalgae contain an important quantity of RubisCO, a photosynthetic enzyme for carbon fixation, with a native protein size between 550 kDa-480 kDa depending on the strain [47]. It was confirmed by Liu et al. that vegetable proteins also contain two protein bands close to 480 kDa (Figure 3.a).

In Figure 3b shows the results of SDS-PAGE for vegetable protein subunits characterization. Compared with the microalgae SDS-PAGE from Teuling et al., 2017, we observed that extracted vegetable protein bands were similar to those of microalgae *Arthrospira sp*. and *Nannochloropsis sp.*, where two bands 55-65 kDa and 10-20 kDa were identified, which could correspond to 8 large subunits and 8 small subunits of Rubisco. Two bands corresponding to units of 40 kDa and 20-30 kDa were also present in microalgae and vegetable proteins. Those results confirmed that vegetable proteins were an acceptable model to represent the microalgae proteins. We can suppose that the interactions between lipids and proteins in the model and real mixtures could be similar.

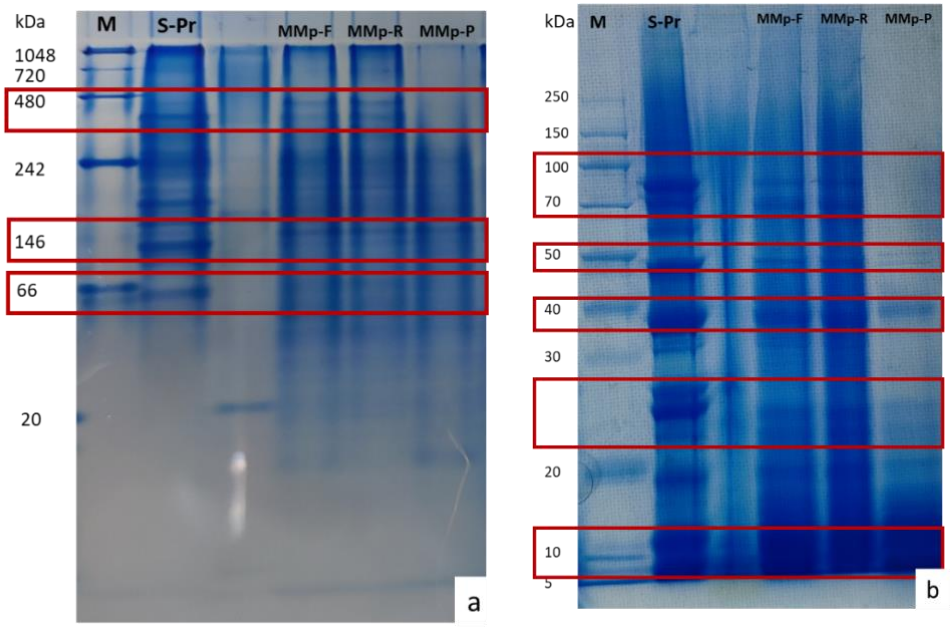

Figure 3. Protein electrophoresis results of extracted soluble vegetable proteins. a: Native-PAGE result from vegetable protein; b: SDS-PAGE results between vegetable protein. (M: marker, S-Pr: extracted soluble vegetable protein, MM_P-F/R/P: feed, retentate or permeate from filtration of MM_P sampled at VRR3)

3.2. Filtration performances studies of the model mixtures and real extracts

In the following paragraphs, the filtration performances (permeation flux and selectivity) are compared for the filtration of the three model and the real microalgae extracts. The analysis complexity is highlighted due to the contrary role of biomolecules on membrane hydrophilisation and fouling. The impact of the lipid-protein interaction on the membrane fouling is demonstrated, its mitigation by shear rate evaluated and the membrane selectivity in the different conditions compared.

3.2.1. Competition between membrane fouling and hydrophilization by the biomolecules

The hydraulic performances of the membrane before, during and after the filtration of model and real mixtures at 30 °C are shown in Table 4 and 5. Due to heterogeneity of membrane porous material, the membrane water flux before concentration experiment ($J_{w\,i}$) ranged from 22 to 61 $L{\cdot}h^{-1}{\cdot}m^{-2}$ for CF and 19 to 66 $L{\cdot}h^{-1}{\cdot}m^{-2}$ for DF.

In CF, considering the membranes with the higher initial water flux (above 30 $L \cdot h^{-1} \cdot m^{-2}$), the filtration of the model mixtures led to a decrease of the permeate flux and the water permeability after rinsing was lower than the initial one. A large quantity of biomolecules probably accumulated on the membrane and blocked pores. For membranes with a lower initial water flux (below 30 $L \cdot h^{-1} \cdot m^{-2}$), the enhancement of the hydrophilicity had a preponderant effect on the permeation, leading to a normalized membrane permeability $J_{MMx} / J_{Wi} > 1$. Thus the evolution of the flux of a given membrane results from a compromise between the membrane hydrophilicity and fouling. In CF, the highest permeation flux was obtained with MM_P.

In DF, regarding the values of the normalized membrane permeability during the concentration process of model mixture $J_{MMx} / J_{W\,i}$ VRR1-3, the flux was always superior to the water flux ($J_{MMx} / J_{W\,i} > 1$). This is coherent with the results from Villafaña-López et al., 2019 [48], even if the authors have worked with a higher shear rate. On the membrane surface, the accumulation of a part of the biomolecules increase the hydrophilicity of the porous material. The partially hydrophobic properties of virgin PES membranes were already described in literature [48–50] and it was already shown on the same membrane K618 (Koch) that polar compounds like proteins could enhance or reduce water permeation depending on the fouling structure [51].

After water rinsing, the final water flux $J_{W\,f}$ was lower than the initial water flux and the filtration flux. It means that the physically reversible fouling made the membrane more hydrophilic, but once it was removed, a residual fouling induced a lower permeability. The impact of this fouling was hidden by the rise of hydrophilicity. Regarding the experiments performed in the same hydrodynamic conditions γ_1 with membrane presenting similar initial water flux (above 30 $L \cdot h^{-1} \cdot m^{-2}$), we observed that the model mixture MM_L, with only 0.15 % of lipids and without proteins, has the highest normalized flux compared to the model mixtures containing proteins. MM_P has the lowest. This implies that the hydrophilization of the membrane by MM_L was improved, probably because of the polar lipids, which adsorbed to the PES polymer, and/or that the fouling by lipids is limited. The polar lipids are smaller and more mobiles than proteins, thus, it is probably easier for them to attach to the membrane surface and to modify the membrane hydrophilicity without blocking the pores.

Regarding the RM, which is 5 times less concentrated (protein and lipids) than the MM, for CF, the permeation flux, the flux ratio J_{RM} / J_{wi} and the J_{Wf} are in the same range as the values obtained with the $MM_{P/L}$ despite the protein and lipid concentration differences. For DF, $J_{RM} /$

466 J_{wi} was still >1 but lower than with the MM. A lower availability of the amphiphilic molecules
467 involved in more complicated aggregates could explain this difference or the rise of membrane
468 fouling due to the presence of other biomolecules like carbohydrates could be the reason.

469

470 *Table 4. Hydraulic performance of the membrane before, during and after CF at 30 °C and 0.45 bar **

N° Assay for CF	$J_{w\,i}$ $L \cdot h^{-1} \cdot m^{-2}$	$J_{w\,f}$ $L \cdot h^{-1} \cdot m^{-2}$	J_{MMx} VRR1-3 $L \cdot h^{-1} \cdot m^{-2}$	J_{MMx} / $J_{W\,i}$ VRR1-3
MM_L	40		39-36	0.9-1.0
MM_L'	61	48	50-51	0.7-0.8
MM_P	44	34	44-43	0.9-1.0
MM_P'	27	32	32-38	1.2-1.4
$MM_{P/L}$	56	58	49-47	0.8-0.9
$MM_{P/L}$'	56	38	44-36	0.6-0.8
$MM_{P/L}$''	22	22	26-25	1.1-1.2
RM	38	44	35-25	0.7-0.9

471 *J_W Membrane water flux before (i) or after (f) concentration experience. J_{MMx} VRR1-3: membrane model mixture
472 flux variation during concentration, values calculated from VRR1 to VRR3. J_{MMx} / $J_{W\,i}$ VRR1-3: model mixture
473 flux normalization with initial membrane water flux. MMx: x represents the composition of the model mixtures,
474 P for proteins and L for lipids. Maximum SD 8% (Apostrophe mark ' and '' means repetition of the experiment)

475

476 *Table 5. Hydraulic performance of the membrane before during and after DF at 30 °C and 0.5bar **

N° Assay for DF	J_{wi} $L \cdot h^{-1} \cdot m^{-2}$	$J_{w\,f}$ $L \cdot h^{-1} \cdot m^{-2}$	J_{MMx} VRR1-3 $L \cdot h^{-1} \cdot m^{-2}$	J_{MMx} / $J_{W\,i}$ VRR1-3
$MM_L\ \gamma_1$	59	53	85-70	1.3-1.5
$MM_L\ \gamma_1$'	44	42	78-67	1.5-1.6
$MM_P\ \gamma_1$	54	39	63-48	1.0-1.2
$MM_P\ \gamma_1$'	19	19	28-27	1.4-1.5
$MM_{P/L}\ \gamma_1$	34	24	52-46	1.0-1.4
$MM_{P/L}\ \gamma_1$'	38	27	61-49	1.3-1.5
$MM_{P/L}\ \gamma_2$	55	41	83-78	1.4-1.6
$MM_{P/L}\ \gamma_2$'	20	16	27-21	1.3-1.5
RM γ_1	66	48	(0.3bar) 44-43	1.0-1.2

477 *J_W Membrane water flux before (i) or after (f) concentration experience. J_{MMx} VRR1-3: membrane model mixture
478 flux variation during concentration, values calculated from VRR1 to VRR3. J_{MMx} / $J_{W\,i}$ VRR1-3: model mixture

flux normalization with initial membrane water flux. MMx: x represents the composition of the model mixtures, P for proteins and L for lipids. Maximum SD 8%. (Apostrophe mark ’ and ’’ means repetition of experiment)

3.2.2. The interaction between lipids and proteins impacts the fouling

Based on the resistance-in-series model, after a water flush, the resistance to water permeation can be estimated as the sum of the clean membrane resistance, the resistance of the physically reversible fouling, the resistance of the chemically reversible fouling, and the resistance of the irreversible fouling [31,32]. Here, the membrane was rinsed with water to remove the physically reversible fouling, thus the fouling resistance R_f represents the total resistance of both chemically reversible fouling and irreversible fouling. It was calculated using the initial water flux and the final water flux after water rinsing, for the coupons with the highest initial water flux (>30 $L \cdot h^{-1} \cdot m^{-2}$) to facilitate comparison. The results are shown in Figure 4. Besides, the lipids accumulated on the membrane after the concentration and water rinsing were quantified by ATR-FTIR analysis (Figure 5).

The impact of the composition of the mixture on the process can be studied by comparing the results of MM_P, MM_L and $MM_{P/L}$ in CF and DF under the same hydrodynamic condition γ_1. The fouling resistance (Figure 4) is higher with proteins (MM_P) than with lipids (MM_L), and this difference is more evident for DF. The proteins seem more likely to generate a fouling, more stable at high shear rate than lipids. MM_P contains protein aggregates and probably free proteins and it can be supposed that both can generate the membrane fouling, with a possible reorganization at the membrane interface.

In the case of $MM_{P/L}$, containing both proteins and lipids, the fouling resistance (figure 4) is higher than with the separated compounds in CF and DF, but it is not the sum of the resistances of lipids alone and proteins alone. A different structure of the fouling occurred. The results of the particle size distribution analysis (Figure 2) in $MM_{P/L}$ suggested a strong reorganization of the proteins, which probably adsorbed at the droplets interface. Thus the droplet interface was modified by proteins. According to the results of ATR-FTIR analysis in Figure 5, comparing MM_L and $MM_{P/L}$ in DF, the addition of proteins in the O/W system led to an increased lipids accumulation on the membrane surface. Thus the presence of proteins modified the behavior of lipids at the membrane surface. They facilitated their accumulation on the membrane and induced a higher resistance. In the case of CF: the quantity of accumulated lipids is the same order of magnitude with or without proteins, but the resistance is different, thus the fouling structure is also different. this array of results leads to the hypothesis that

proteins interacted with lipids, induced a stronger adsorption of lipids on the membrane (the lipids can not be removed by dynamic filtration when proteins are present) and that it had a negative impact on the permeability of the membrane filtration (higher fouling resistance).

3.2.3. The role of the shear rate on the fouling mitigation

Comparing the CF and DF γ_1 resistance, it appears that with MM_L, R_f in CF is higher than R_f in DF, showing that the higher shear rate is useful to eliminate the lipid fouling.

In presence of proteins, with MM_P and $MM_{P/L}$, the fouling resistance becomes higher in DF than in CF. The shear rate may induce a different structure of the fouling (enhanced internal fouling or denser fouling for example) leading to a lower permeability. Concerning the impact of hydrodynamic conditions γ_2 on filtration performances, the fouling resistance (Figure 4) R_f of $MM_{P/L}$ DF γ_2 is almost twice lower than $MM_{P/L}$ γ_1 and R_f of $MM_{P/L}$ CF is in between. The hydrodynamic has two different impacts: the potential removal of the fouling but also the modification of its structure, leading to a positive or negative effect on the permeation depending on the filtrated product. The results of ATR-FTIR analysis also confirmed that the lipid accumulation on the membrane surface for $MM_{P/L}$ DF γ_1 (analysis at medium position: 400 $\mu g \cdot cm^{-2}$) was much higher than in CF (170 $\mu g \cdot cm^{-2}$) and DF γ_2 (analysis at medium position: 40 $\mu g \cdot cm^{-2}$)).

The role of hydrodynamics is also highlighted for each DF experiment in figure 5. The rotation of the disc creates a shear rate stronger on the periphery of the membrane than near the center, which moves the lipids fouling deposit more efficiently from the periphery than from the center of the membrane. Goh et al., 2018; Zhang et al., 2015 and Zhang and Ding, 2015 [52–54] also confirmed that shear-enhanced dynamic filtration effectively prevented the deposition of substances on the membrane surface.

Based on these results the hypothesis is that at low shear rate (CF), the fouling can settle but has a limited impact on the flux, thanks to an open structure. When the shear rate is higher (DF γ_1), a different fouling organizes, which can be strongly lowered if the shear rate is high enough (DF γ_2).

Comparing RM filtration in CF and DF, results are different. In CF, the filtration flux is similar to the $MM_{P/L}$ but fouling resistance was negative even if lipids accumulated in the same

range (250 µg·cm^{-2}). The hydrophilization of the membrane offsets the fouling impact and the hydrophilic molecules were not removed by water rinsing. This may be due to carbohydrates present in RM. In DF, the flux with RM is lower than with $MM_{P/L}$, but after rinsing, the fouling resistance is smaller and the quantity of lipids the same order of magnitude. It means that the physically reversible fouling is preponderant in this case.

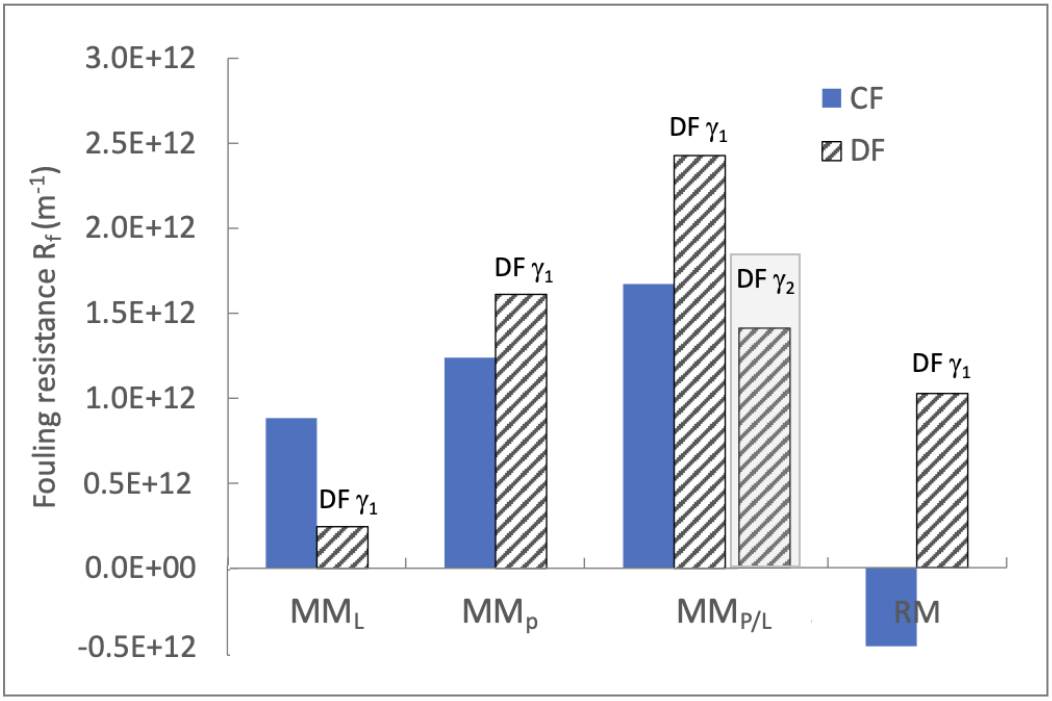

Figure 4. Fouling resistance (R_f) of different mixtures in CF and DF under two hydrodynamic conditions (γ_1 and γ_2 – highlighted in light gray)

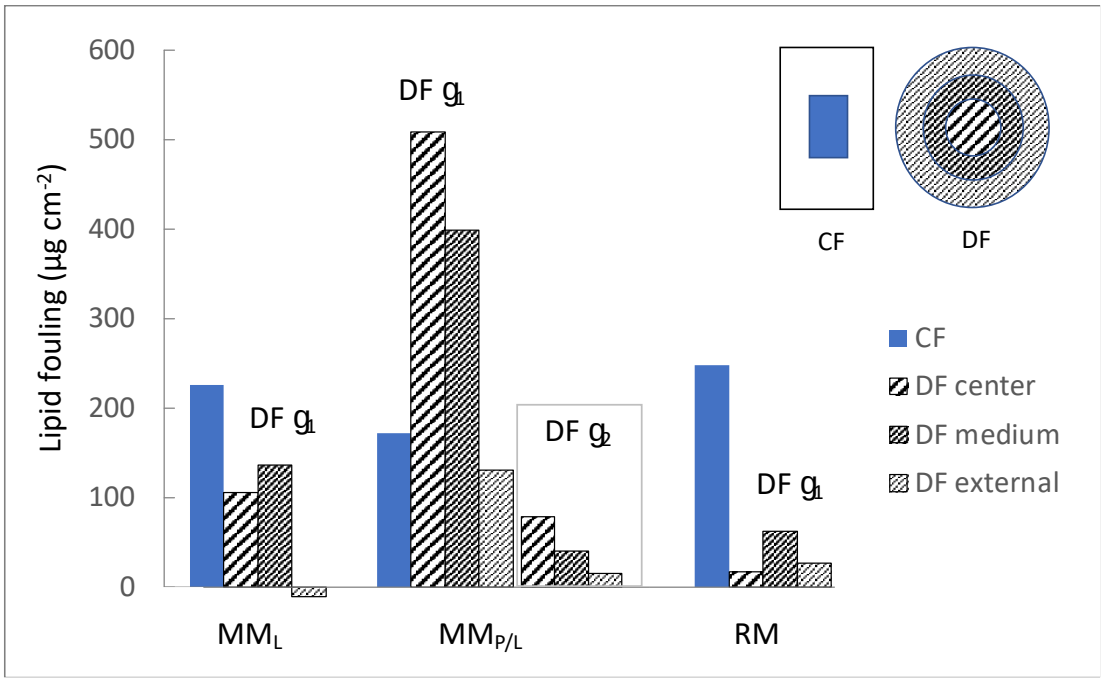

Figure 5. Lipids membrane fouling characterization by ATR-FTIR analysis for model (MM) and real (RM) mixtures. The lipids were quantified in the center of the cross-flow membrane (CF) and in the center, intermediate and external annular bands of the dynamic filtration membrane (DF), for two different shear rates (γ_1 at 16 000 s^{-1} and γ_2 66 000 s^{-1} -highlighted in light gray).

3.2.4. Membrane selectivity

Table 6 presents the retention rates of total dry matter (DM), proteins and lipids. Firstly, we observe a total lipid retention for both model and real mixtures, which means the concentration of lipids from microalgae extract by membrane process is efficient. For proteins, different retention rates were observed.

During the filtration of MM_P, 57-77 % of protein retention rate were obtained in CF and DF. An important part of proteins aggregated as shown in Figure 2, but 23 – 41 % of proteins were probably free and passed through the membrane with a MWCO 0.1 µm. The free proteins were not visible in the volume size distribution due to the presence of large aggregates. But the Native-PAGE electrophoresis results (Figure 3) show that proteins smaller than 240 kDa could pass through the membrane (MMp-P). According to SDS-PAGE electrophoresis, they contain mostly subunits below 50 kDa but unfortunately this information did not allow any protein identification.

In the presence of lipids ($MM_{P/L}$ filtration), the retention rate of proteins increased to 78-84% in CF and DF, whereas the aggregates characterized were smaller. This means that a part of the soluble proteins, which should permeate through the membrane, were retained at the

membrane interface and were not free anymore. The fouling contained more lipids than MM_L (Figure 5) but also probably more proteins.

Besides, according to Courthaudon et al., 1991.; Damodaran, 2005 and Euston et al., 1995 [21,43,44], when lecithin and protein-based emulsifiers are mixed before emulsification process, those molecules compete with each other for the adsorption on the oil-water interface and form multi-emulsifier micelles. This competitive adsorption can vary with the ratio of two emulsifiers, and in our case, for $MM_{P/L}$, the amount of proteins-based emulsifier is much more important than lecithin. Dickinson, 2001 [55] reported that the protein conformations around the oil droplet are generally more stable than that of a small surfactant. In particular, the sulfhydryl and disulfide groups in proteins make them irreversibly adsorbed to the oil-water interface, creating a highly viscoelastic film. This may be the reason of the increased protein retention rate in $MM_{P/L}$ and RM.

Accordingly, for real mixture filtration, it is interesting to compare our results with those of Kulkarni and Nikolov, 2018 and Ursu et al., 2014 [17,19]. All of them filtered the supernatant from *Chlorella vulgaris* after cell disruption by HPH and clarification, with a membrane PES 300 kDa using tangential filtration, under neutral pH conditions, similar protein retention was reported (80-87 %). We could have expected more protein transmission with the larger MWCO used in this work but it was not the case.

Comparing the retention rate of proteins and lipids ($RR_{proteins}$ and RR_{lipids}) between $MM_{P/L}$ γ_1 and RM γ_1, no significant difference was observed, the difference in retention of DM is due to the presence of a large amount of carbohydrates in RM (0.72 $g \cdot L^{-1}$).

Regarding the effect of hydrodynamic conditions on the membrane selectivity, comparing $MM_{P/L}$ γ_1 and $MM_{P/L}$ γ_2, no significant difference in retention rates (proteins and lipids) was observed. Thus, these results confirm that higher shear force favors an increase in flux and therefore productivity, but does not increase membrane selectivity. The aggregates containing lipids and proteins seem very stable and large enough to be retained.

Table 6. Dry matter (DM), proteins and lipids retention rate (RR) at VRR3 for different model mixtures and real mixture

	CF			DF		
N° Assay	RR_{DM}	$RR_{proteins}$	RR_{lipids}	RR_{DM}	$RR_{Proteins}$	RR_{Lipids}
	%	%	%	%	%	%
$MM_L\ \gamma_1$	/	/	100	89.6±3.9	/	100
$MM_L\ \gamma_1$'	87.8±5.0	/	100	83.3±8.5	/	100
$MM_P\ \gamma_1$	44.4±6.6	/	/	31.7±1.2	58.8±3.0	/
$MM_P\ \gamma_1$'	22.8±0.4	57.0±1.6	/	55.9±1.3	77.0±1.2	/
$MM_{P/L}\ \gamma_1$	85.3±1.9	82.3±2.1	100	78.4±1.2	84.7±2.7	100
$MM_{P/L}\ \gamma_1$'	80.7±5.9	77.9±1.4	100	79.7±1.2	80.5±0.9	100
$MM_{P/L}\ \gamma_2$	78.3±2.4	74.5±3.3	100	82.3±6.5	81.0±4.1	100
$MM_{P/L}\ \gamma_2$'	/	/	/	85.7±0.8	92.3±2.9	100
RM γ_1	66.5±6.6	84.5±0.8	100	63.2±6.5	86.0±1.2	100

* MMx: x represents the composition of the model mixtures, P for proteins and L for lipids. (Apostrophe mark ' and '' means repetition of experiment)

4. Conclusion

The microalgae biorefining necessitates the coupling of cell disruption and separation operation units. The intrinsic microalgae composition or the cell disruption was supposed to generate interactions between biomolecules that can hinder the separation. The objective in this work was to evaluate more specifically the impact of the lipids and proteins interaction on their separation by microfiltration. Through the formulation of three representative model mixtures containing lipids, proteins or both kinds of molecules, their filtration and comparison with real microalgae extracts, it was demonstrated that the strong interaction between the biomolecules in solution had a deep impact on filtration performances: the membrane fouling worsens and the productivity and selectivity are limited. The dynamic filtration was tested to enhance the performances compared to cross-flow filtration. The higher shear rate favored an increase in flux and therefore productivity, but did not modify membrane selectivity. The concentration of lipids was possible, with a total retention of lipids, but their interaction with proteins induced a higher fouling, and limited the protein permeation. The results obtained with the lipids and proteins mixture were similar to the real mixtures thus bringing a part of understanding on the limitation met with microalgae extracts. It was therefore demonstrated that the interaction between molecules drives the separation efficiency and should be mitigated before filtration in future works to allow the whole biomass biorefining.

Acknowledgments and financial support

This work was supported by the French Environment and Energy Management Agency (ADEME), the French region of Pay de la Loire, the Challenge Food For Tomorrow/Cap Aliment, Pays de la Loire, France (project 3MFOODGY) and the Process Engineering for Environment and Food Laboratory (GEPEA), University of Nantes (France).

No conflicts, informed consent, or human or animal rights are applicable to this study.

Authorship contributions: E. Couallier, M. Frappart and S. Liu were responsible for the conception and design of the study. The data were acquired by S. Liu, C. Rouquié and M. Rabiller Baudry. The data were analyzed and interpreted and the manuscript written by E. Couallier, S. Liu, M. Rabiller Baudry, A. Szymczyk C. Rouquié and M. Frappart. All the authors approved the final manuscript.

References:

[1] R. Halim, B. Gladman, M.K. Danquah, P.A. Webley, Oil extraction from microalgae for biodiesel production, Bioresource Technology. 102 (2011) 178–185. https://doi.org/10.1016/j.biortech.2010.06.136.

[2] A. Melis, Photosynthetic H2 metabolism in Chlamydomonas reinhardtii (unicellular green algae), Planta. 226 (2007) 1075–1086. https://doi.org/10.1007/s00425-007-0609-9.

[3] M.L. Mourelle, C.P. Gómez, J.L. Legido, The Potential Use of Marine Microalgae and Cyanobacteria in Cosmetics and Thalassotherapy, Cosmetics. 4 (2017) 46. https://doi.org/10.3390/cosmetics4040046.

[4] O. Pulz, W. Gross, Valuable products from biotechnology of microalgae, Appl Microbiol Biotechnol. 65 (2004) 635–648. https://doi.org/10.1007/s00253-004-1647-x.

[5] V. Yusibov, N. Kushnir, S.J. Streatfield, Antibody Production in Plants and Green Algae, Annu. Rev. Plant Biol. 67 (2016) 669–701. https://doi.org/10.1146/annurev-arplant-043015-111812.

[6] B. Fernandes, J. Teixeira, G. Dragone, A.A. Vicente, S. Kawano, K. Bišová, P. Přibyl, V. Zachleder, M. Vítová, Relationship between starch and lipid accumulation induced by nutrient depletion and replenishment in the microalga Parachlorella kessleri, Bioresource Technology. 144 (2013) 268–274. https://doi.org/10.1016/j.biortech.2013.06.096.

[7] R. Kandilian, A. Taleb, V. Heredia, G. Cogne, J. Pruvost, Effect of light absorption rate and nitrate concentration on TAG accumulation and productivity of Parachlorella kessleri cultures grown in chemostat mode, Algal Research. 39 (2019) 101442. https://doi.org/10.1016/j.algal.2019.101442.

[8] A. Taleb, R. Kandilian, R. Touchard, V. Montalescot, T. Rinaldi, S. Taha, H. Takache, L. Marchal, J. Legrand, J. Pruvost, Screening of freshwater and seawater microalgae strains in fully controlled photobioreactors for biodiesel production, Bioresource Technology. 218 (2016) 480–490. https://doi.org/10.1016/j.biortech.2016.06.086.

[9] G.P. Tlam, M.H. Vermuë, M.H.M. Eppink, R.H. Wijffels, C. van den Berg, Multi-Product Microalgae Biorefineries: From Concept Towards Reality, Trends in Biotechnology. 36 (2018) 216–227. https://doi.org/10.1016/j.tibtech.2017.10.011.

[10] E. Clavijo Rivera, Etude physicochimique du comportement d'une solution synthétique d'un broyat de microalgues et de la séparation par procédés membranaires des lipides qu'il contient, thesis, Nantes, 2017. http://www.theses.fr/2017NANT4099 (accessed June 3, 2019).

[11] V. Montalescot, Contribution au bioraffinage de microalgues oléagineuses: impact de la destruction cellulaire sur le fractionnement en voie humide des composés intracellulaires., Université de Nantes, 2016.

[12] J.-Y. Park, M.S. Park, Y.-C. Lee, J.-W. Yang, Advances in direct transesterification of algal oils from wet biomass, Bioresource Technology. 184 (2015) 267–275. https://doi.org/10.1016/j.biortech.2014.10.089.

[13] S. Liu, I. Gifuni, H. Mear, M. Frappart, E. Couallier, Recovery of soluble proteins from Chlorella vulgaris by bead-milling and microfiltration: Impact of the concentration and the physicochemical conditions during the cell disruption on the whole process, Process Biochemistry. (2021). https://doi.org/10.1016/j.procbio.2021.05.021.

[14] P.R. Postma, G. Pataro, M. Capitoli, M.J. Barbosa, R.H. Wijffels, M.H.M. Eppink, G. Olivieri, G. Ferrari, Selective extraction of intracellular components from the microalga Chlorella vulgaris by combined pulsed electric field–temperature treatment, Bioresource Technology. 203 (2016) 80–88. https://doi.org/10.1016/j.biortech.2015.12.012.

[15] P. Aimar, P. BACCHIN, A. MAUREL, Filtration membranaire (OI, NF, UF, MFT) - Aspects théoriques : perméabilité et sélectivité, Ref : TIP452WEB - "Opérations unitaires. Génie de la réaction chimique." (2010). https://www.techniques-ingenieur.fr/base-documentaire/procedes-chimie-bio-agro-th2/operations-unitaires-techniques-separatives-sur-membranes-42331210/filtration-membranaire-oi-nf-uf-mft-j2790/ (accessed January 25, 2021).

[16] Z. Berk, Chapter 10 - Membrane processes, in: Z. Berk (Ed.), Food Process Engineering and Technology, Academic Press, San Diego, 2009: pp. 233–257. https://doi.org/10.1016/B978-0-12-373660-4.00010-7.

[17] S. Kulkarni, Z. Nikolov, Process for selective extraction of pigments and functional proteins from Chlorella vulgaris, Algal Research. 35 (2018) 185–193. https://doi.org/10.1016/j.algal.2018.08.024.

[18] C. Safi, L. Cabas Rodriguez, W.J. Mulder, N. Engelen-Smit, W. Spekking, L.A.M. van den Broek, G. Olivieri, L. Sijtsma, Energy consumption and water-soluble protein release by cell wall disruption of Nannochloropsis gaditana, Bioresource Technology. 239 (2017) 204–210. https://doi.org/10.1016/j.biortech.2017.05.012.

[19] A.-V. Ursu, A. Marcati, T. Sayd, V. Sante-Lhoutellier, G. Djelveh, P. Michaud, Extraction, fractionation and functional properties of proteins from the microalgae Chlorella vulgaris, Bioresource Technology. 157 (2014) 134–139. https://doi.org/10.1016/j.biortech.2014.01.071.

[20] R. Aveyard, B.P. Binks, J.H. Clint, Emulsions stabilised solely by colloidal particles, Advances in Colloid and Interface Science. 100–102 (2003) 503–546. https://doi.org/10.1016/S0001-8686(02)00069-6.

[21] S. Damodaran, Protein Stabilization of Emulsions and Foams, Journal of Food Science. 70 (2005) R54–R66. https://doi.org/10.1111/j.1365-2621.2005.tb07150.x.

[22] E. Clavijo Rivera, V. Montalescot, M. Viau, D. Drouin, P. Bourseau, M. Frappart, C. Monteux, E. Couallier, Mechanical cell disruption of Parachlorella kessleri microalgae: Impact on lipid fraction composition, Bioresource Technology. 256 (2018) 77–85. https://doi.org/10.1016/j.biortech.2018.01.148.

[23] P. Bertsch, L. Böcker, A. Mathys, P. Fischer, Proteins from microalgae for the stabilization of fluid interfaces, emulsions, and foams, Trends in Food Science & Technology. 108 (2021) 326–342. https://doi.org/10.1016/j.tifs.2020.12.014.

[24] C. Acquah, Y. Zhang, M.A. Dubé, C.C. Udenigwe, Formation and characterization of protein-based films from yellow pea (Pisum sativum) protein isolate and concentrate for edible applications, Current Research in Food Science. 2 (2020) 61–69. https://doi.org/10.1016/j.crfs.2019.11.008.

[25] D. Cd, G. S, Formation and Stability of Pea Proteins Nanoparticles Using Ethanol-Induced Desolvation., Nanomaterials (Basel). 9 (2019). https://doi.org/10.3390/nano9070949.

[26] Malvern Panalytical, Laser diffraction Masterclass 4: Optical properties | Malvern Panalytical, (n.d.). https://www.malvernpanalytical.com/fr/learn/events-and-

721 training/webinars/W130716LaserDiffractionMasterclass4Optical (accessed November
722 20, 2020).

723 [27] Q. Ye, M. Biviano, S. Mettu, M. Zhou, R. Dagastine, M. Ashokkumar, Modification of
724 pea protein isolate for ultrasonic encapsulation of functional liquids, RSC Advances. 6
725 (2016) 106130–106140. https://doi.org/10.1039/C6RA17585F.

726 [28] J. Vörös, The Density and Refractive Index of Adsorbing Protein Layers, Biophysical
727 Journal. (n.d.) 9.

728 [29] M. Frappart, A. Massé, M.Y. Jaffrin, J. Pruvost, P. Jaouen, Influence of hydrodynamics
729 in tangential and dynamic ultrafiltration systems for microalgae separation, Desalination.
730 265 (2011) 279–283. https://doi.org/10.1016/j.desal.2010.07.061.

731 [30] R. Bouzerar, L. Ding, M.Y. Jaffrin, Local permeate flux–shear–pressure relationships in
732 a rotating disk microfiltration module: implications for global performance, Journal of
733 Membrane Science. 170 (2000) 127–141. https://doi.org/10.1016/S0376-7388(99)00348-
734 8.

735 [31] M. Rabiller-Baudry, A. Bouzin, C. Hallery, J. Girard, C. Leperoux, Evidencing the
736 chemical degradation of a hydrophilised PES ultrafiltration membrane despite protein
737 fouling, Separation and Purification Technology. 147 (2015) 62–81.
738 https://doi.org/10.1016/j.seppur.2015.03.056.

739 [32] C. Rouquié, A. Szymczyk, M. Rabiller-Baudry, H. Roberge, P. Abellan, A. Riaublanc, M.
740 Frappart, S. Álvarez-Blanco, E. Couallier, NaCl precleaning of microfiltration membranes
741 fouled with oil-in-water emulsions: Impact on fouling dislodgment, Separation and
742 Purification Technology. 285 (2022) 120353.
743 https://doi.org/10.1016/j.seppur.2021.120353.

744 [33] D. Delaunay, M. Rabiller-Baudry, J.M. Gozálvez-Zafrilla, B. Balannec, M. Frappart, L.
745 Paugam, Mapping of protein fouling by FTIR-ATR as experimental tool to study
746 membrane fouling and fluid velocity profile in various geometries and validation by CFD
747 simulation, Chemical Engineering and Processing: Process Intensification. 47 (2008)
748 1106–1117. https://doi.org/10.1016/j.cep.2007.12.008.

749 [34] E. Clavijo Rivera, L. Villafaña-López, S. Liu, R. Vinoth Kumar, M. Viau, P. Bourseau,
750 C. Monteux, M. Frappart, E. Couallier, Cross-flow filtration for the recovery of lipids from
751 microalgae aqueous extracts: Membrane selection and performances, Process
752 Biochemistry. 89 (2020) 199–207. https://doi.org/10.1016/j.procbio.2019.10.016.

753 [35] B. Ozturk, D.J. McClements, Progress in natural emulsifiers for utilization in food
754 emulsions, Current Opinion in Food Science. 7 (2016) 1–6.
755 https://doi.org/10.1016/j.cofs.2015.07.008.

756 [36] H. Hoffmann, M. Reger, Emulsions with unique properties from proteins as emulsifiers,
757 Adv Colloid Interface Sci. 205 (2014) 94–104. https://doi.org/10.1016/j.cis.2013.08.007.

758 [37] E.W. Becker, Micro-algae as a source of protein, Biotechnology Advances. 25 (2007)
759 207–210. https://doi.org/10.1016/j.biotechadv.2006.11.002.

760 [38] A.C. Karaca, N. Low, M. Nickerson, Emulsifying properties of chickpea, faba bean, lentil
761 and pea proteins produced by isoelectric precipitation and salt extraction, Food Research
762 International. 44 (2011) 2742–2750. https://doi.org/10.1016/j.foodres.2011.06.012.

763 [39] R.S.H. Lam, M.T. Nickerson, Food proteins: A review on their emulsifying properties
764 using a structure–function approach, Food Chemistry. 141 (2013) 975–984.
765 https://doi.org/10.1016/j.foodchem.2013.04.038.

[40] A. Taleb, Production de biodiesel à partir des microalgues : recherche des souches accumulatrices des lipides et optimisation des conditions de culture en photobioréacteurs, These de doctorat, Nantes, 2015. https://www.theses.fr/2015NANT2007 (accessed August 29, 2023).

[41] M.B. Linder, Hydrophobins: Proteins that self assemble at interfaces, Current Opinion in Colloid & Interface Science. 14 (2009) 356–363. https://doi.org/10.1016/j.cocis.2009.04.001.

[42] A. Stradner, H. Sedgwick, F. Cardinaux, W.C.K. Poon, S.U. Egelhaaf, P. Schurtenberger, Equilibrium cluster formation in concentrated protein solutions and colloids, Nature. 432 (2004) 492–495. https://doi.org/10.1038/nature03109.

[43] J.-L. Courthaudon, E. Dickinson, Y. Matsumura, A. Williams, Influence of Emulsifier on the Competitive Adsorption of Whey Proteins in Emulsions, Food Structure. 10 (1991) 109–115.

[44] S.E. Euston, H. Singh, P.A. Munro, D.G. Dalgleish, Competitive Adsorption Between Sodium Caseinate and Oil-Soluble and Water-Soluble Surfactants in Oil-in-Water Emulsions, Journal of Food Science. 60 (1995) 1124–1131. https://doi.org/10.1111/j.1365-2621.1995.tb06307.x.

[45] R.S. Alavijeh, K. Karimi, R.H. Wijffels, C. van den Berg, M. Eppink, Combined bead milling and enzymatic hydrolysis for efficient fractionation of lipids, proteins, and carbohydrates of Chlorella vulgaris microalgae, Bioresource Technology. 309 (2020) 123321. https://doi.org/10.1016/j.biortech.2020.123321.

[46] E. Günerken, E. D'Hondt, M. Eppink, K. Elst, R. Wijffels, Influence of nitrogen depletion in the growth of N. oleoabundans on the release of cellular components after beadmilling, Bioresource Technology. 214 (2016) 89–95. https://doi.org/10.1016/j.biortech.2016.04.072.

[47] E. Teuling, P.A. Wierenga, J.W. Schrama, H. Gruppen, Comparison of Protein Extracts from Various Unicellular Green Sources, Journal of Agricultural and Food Chemistry. 65 (2017) 7989–8002. https://doi.org/10.1021/acs.jafc.7b01788.

[48] L. Villafaña-López, E. Clavijo Rivera, S. Liu, E. Couallier, M. Frappart, Shear-enhanced membrane filtration of model and real microalgae extracts for lipids recovery in biorefinery context, Bioresource Technology. 288 (2019) 121539. https://doi.org/10.1016/j.biortech.2019.121539.

[49] N. Wemsy Diagne, M. Rabiller-Baudry, L. Paugam, On the actual cleanability of polyethersulfone membrane fouled by proteins at critical or limiting flux, Journal of Membrane Science. 425–426 (2013) 40–47. https://doi.org/10.1016/j.memsci.2012.09.001.

[50] N. Mahdi, P. Kumar, A. Goswami, B. Perdicakis, K. Shankar, M. Sadrzadeh, Robust Polymer Nanocomposite Membranes Incorporating Discrete TiO2 Nanotubes for Water Treatment, Nanomaterials. 9 (2019) 1186. https://doi.org/10.3390/nano9091186.

[51] S. Habibi, M. Rabiller-Baudry, F. Lopes, F. Bellet, B. Goyeau, M. Rakib, E. Couallier, New insights into the structure of membrane fouling by biomolecules using comparison with isotherms and ATR-FTIR local quantification, Environmental Technology. 43 (2020) 207–224. https://doi.org/10.1080/09593330.2020.1783370.

809 [52] P.S. Goh, W.J. Lau, M.H.D. Othman, A.F. Ismail, Membrane fouling in desalination and
810 its mitigation strategies, Desalination. 425 (2018) 130–155.
811 https://doi.org/10.1016/j.desal.2017.10.018.

812 [53] W. Zhang, N. Grimi, M.Y. Jaffrin, L. Ding, Leaf protein concentration of alfalfa juice by
813 membrane technology, Journal of Membrane Science. 489 (2015) 183–193.
814 https://doi.org/10.1016/j.memsci.2015.03.092.

815 [54] W. Zhang, L. Ding, Investigation of membrane fouling mechanisms using blocking
816 models in the case of shear-enhanced ultrafiltration, Separation and Purification
817 Technology. 141 (2015) 160–169. https://doi.org/10.1016/j.seppur.2014.11.041.

818 [55] E. Dickinson, Milk protein interfacial layers and the relationship to emulsion stability and
819 rheology, Colloids and Surfaces B: Biointerfaces. 20 (2001) 197–210.
820 https://doi.org/10.1016/S0927-7765(00)00204-6.

821